



HAL
open science

Rhabdomyosarcoma targeting with tuned porous silicon nanoparticles

Sofia Dominguez-Gil, Rita Sala, Victoria Judith Morel, Christophe Nguyen, Khaled El Cheikh, Alain Morère, Jean-Olivier Durand, Jochen Rössler, Michele Bernasconi, Frédérique Cunin, et al.

► **To cite this version:**

Sofia Dominguez-Gil, Rita Sala, Victoria Judith Morel, Christophe Nguyen, Khaled El Cheikh, et al.. Rhabdomyosarcoma targeting with tuned porous silicon nanoparticles. *Nano Select*, 2024, 5 (7-8), 10.1002/nano.202400004 . hal-04696552

HAL Id: hal-04696552

<https://hal.science/hal-04696552v1>

Submitted on 2 Dec 2024

HAL is a multi-disciplinary open access archive for the deposit and dissemination of scientific research documents, whether they are published or not. The documents may come from teaching and research institutions in France or abroad, or from public or private research centers.

L'archive ouverte pluridisciplinaire **HAL**, est destinée au dépôt et à la diffusion de documents scientifiques de niveau recherche, publiés ou non, émanant des établissements d'enseignement et de recherche français ou étrangers, des laboratoires publics ou privés.



Distributed under a Creative Commons Attribution 4.0 International License

RESEARCH ARTICLE

Rhabdomyosarcoma targeting with tuned porous silicon nanoparticles

Sofia Dominguez-Gil¹ | Rita Sala² | Victoria Judith Morel² | Christophe Nguyen³ | Khaled El Cheikh⁴ | Alain Morère³ | Jean-Olivier Durand¹ | Jochen Rössler^{2,5} | Michele Bernasconi^{2,5} | Frédérique Cunin¹  | Magali Gary-Bobo³

¹Université de Montpellier, ICGM, CNRS, ENSCM, Montpellier, France

²Department of Pediatric Hematology and Oncology, Inselspital, Bern University Hospital, University of Bern, Bern, Switzerland

³Université de Montpellier, IBMM, CNRS, ENSCM, Montpellier, France

⁴Université de Montpellier, NanoMedSyn, Montpellier, France

⁵Translational Cancer Research, Department for BioMedical Research (DBMR), University of Bern, Bern, Switzerland

Correspondence

Michele Bernasconi, Department of Pediatric Hematology and Oncology, Inselspital, Bern University Hospital, University of Bern, 3010, Bern, Switzerland.

Email: michele.bernasconi@unibe.ch

Frédérique Cunin, Université de Montpellier, ICGM, CNRS, ENSCM, Montpellier, France.

Email: frederique.cunin@enscm.fr

Magali Gary-Bobo, Université de Montpellier, IBMM, CNRS, ENSCM, Montpellier, France.

Email: magali.gary-bobo@inserm.fr

Funding information

French National Research Agency, Grant/Award Number: ANR-10-INBS-04; NETPORE, Grant/Award Number: CA20126; COST (European Cooperation in Science and Technology); Université de Montpellier; Bernese Foundation for Children and Young Adults with Cancer; Mach-Gaensslen Foundation

Abstract

We describe porous silicon nanoparticles (pSiNP) chemically functionalized with an analog of mannose 6-phosphate (AMFA) and a porphyrin derivative to target aggressive pediatric Rhabdomyosarcoma (RMS) tumor cells. Our findings demonstrate that the pSiNP@AMFA@porphyrin nanosystems are efficiently internalized by RMS cells, which overexpress mannose 6-phosphate receptors, and induce cytotoxicity and phototoxicity when exposed to two-photon excitation light. These results provide an interesting potential for targeting and treating RMS pediatric tumors.

KEYWORDS

mannose 6-phosphate receptor, porous silicon nanoparticles, Rhabdomyosarcoma targeting, two-photon excitation photodynamic therapy

1 | INTRODUCTION

Rhabdomyosarcoma (RMS) is the most common soft tissue sarcoma in children,^[1] two main subtypes:

Sofia Dominguez-Gila, Rita Salab, and Victoria Judith Morel contributed equally to this work.

This is an open access article under the terms of the [Creative Commons Attribution](https://creativecommons.org/licenses/by/4.0/) License, which permits use, distribution and reproduction in any medium, provided the original work is properly cited.

© 2024 The Author(s). *Nano Select* published by Wiley-VCH GmbH.

embryonic RMS (eRMS; 60–70%) and alveolar RMS (aRMS; 20–30%).^[2] The aggressive aRMS tumors carry one of two characteristic chromosomal translocations, t(2;13)(q35;q14) or t(1;13)(p36;q14) that result in the expression of PAX3::FOXO1 or PAX7::FOXO1 fusion transcription factor, respectively,^[3] and are now classified as fusion-positive (FP) RMS. Embryonal RMS tumors have a better prognosis and are clinically indistinguishable from fusion-negative (FN) RMS.^[4] Surgery, chemotherapy, and radiotherapy are the main therapeutic approaches to treat local and metastatic disease. Over the past decades overall survival has improved significantly reaching up to 70%.^[5] However, for high risk and metastatic RMS, survival rates are still very low.^[6] Moreover, the aggressive chemotherapy and radiation therapy regimens affect the quality of life of children under treatment^[7] and cause long-term toxicities.^[8–10] Therefore, development of novel effective targeted strategies, not only to increase survival but also to decrease the long-term side effects, is urgently needed for children and young adults with high-risk and recurrent solid tumors.

Increasing therapeutic response while reducing side effects can be realized by using nanoparticles as drug carriers for selective drug uptake.^[11] Multiple technologies have been explored, such as liposomes,^[12] polymeric,^[13] and inorganic nanoparticles.^[14] Several of these have reached the clinical testing phase also for pediatric tumors.^[15] In addition, the association of two-photon excitation photodynamic therapy (TPE-PDT) and nanoparticles offers several advantages in the treatment of cancer among other illnesses, being nowadays an important research area in cancer treatments. On one hand, PDT consists of using a photosensitizer (PS),^[16] which is administered either systemically, locally, or topically, and illuminated with appropriate irradiation. Under irradiation, the PS transfers its energy to the surrounding oxygen (in its triplet state) which generates singlet oxygen and other cytotoxic species, leading to cell death,^[17] PDT allows a more localized and less invasive treatment diminishing the side effects induced by conventional treatments. On the other hand, the employment of nanoparticles allows to overcome some inherent limitations of the PS used in PDT such as poor pharmacokinetic profile and low specificity for tumors. Then, the use of NPs as vehicles can protect the PS during systemic circulation and facilitate the selective accumulation at the tumor site.^[18] Gold nanorods are examples of inorganic nanoparticles used in TPE-PDT,^[19,20] however, they present limitations in terms of toxicity^[16–18] and non-biodegradability.^[21,22] Porous silicon nanoparticles (pSiNP) emerged as an appropriate substitute because they have already shown their suitability for other biological applications such as drug delivery,^[23] and can be excited with two-photon near

infrared light which penetrates tissues deeper.^[24] Xiao et al. first showed the use of pSiNP for singlet oxygen production and PDT. After irradiating HeLa and NIH-3T3 cells incubated with pSiNP with a 60 J cm⁻² white light for 10 minutes, a 45% cell death was observed. Control assay with the same cells in absence of nanoparticles showed between 10% and 25% of cell death.^[25] Nevertheless, the PDT efficacy could be improved not only by the attachment of PSs to the nanoparticles, inducing an increase in the singlet oxygen generation, but also by grafting targeting molecules to specifically target the malignant tissue. Secret et al. described nanosystems that consist of pSiNP covalently functionalized with porphyrins and mannose as a targeting molecule, resulting in a better cell-killing effect compared to the use of free porphyrin and non-targeting nanoparticles. In this case, the pSiNP were irradiated under two-photon excitation light in the near Infra-Red and were able to transfer part of their energy to the porphyrin via a resonant energy transfer mechanism.^[26]

Herein, we describe the functionalization of the pSiNP with an analogue of mannose 6-phosphate functionalized on anomeric position (AMFA) and a porphyrin derivative. We also discuss the photodynamic efficacy of the formulations in TPE-PDT on two different RMS cell lines. Our hypothesis is that the employment of pSiNP@AMFA@porphyrin will improve the TPE-PDT effectiveness due to both: the AMFA, which favors the internalization of pSiNP via mannose-6-phosphate receptors (M6PR) overexpressed in RMS cells^[27] and the energy transfer between the pSiNP and the porphyrin, which induces the ROS production.

2 | RESULTS AND DISCUSSION

Bare pSiNP were synthesized according to the protocol described in the experimental section, by anodization of a crystalline silicon wafer, followed by film lifting-off and ultrasound treatment. The rationale for using pSiNP made by electrochemical etching of highly doped crystalline silicon is to obtain nanoparticles with control of their textural and optical properties. The pSiNP described in this work display a large surface area and available porous volume, allowing for increased surface chemical functionalization and encapsulation possibilities, compared to low-grade (ground/milled) non-porous solid silicon nanoparticles, and with a much better control of their biodegradation rate.^[26] The obtained pSiNP exhibited a negative zeta potential value of -38.8 ± 0.2 mV (NaCl 1 mM, pH 7.2), due to the silanol groups present on their surface. Subsequently, allylamine was grafted by hydrosilylation onto the surface as well as inside the pores following a procedure

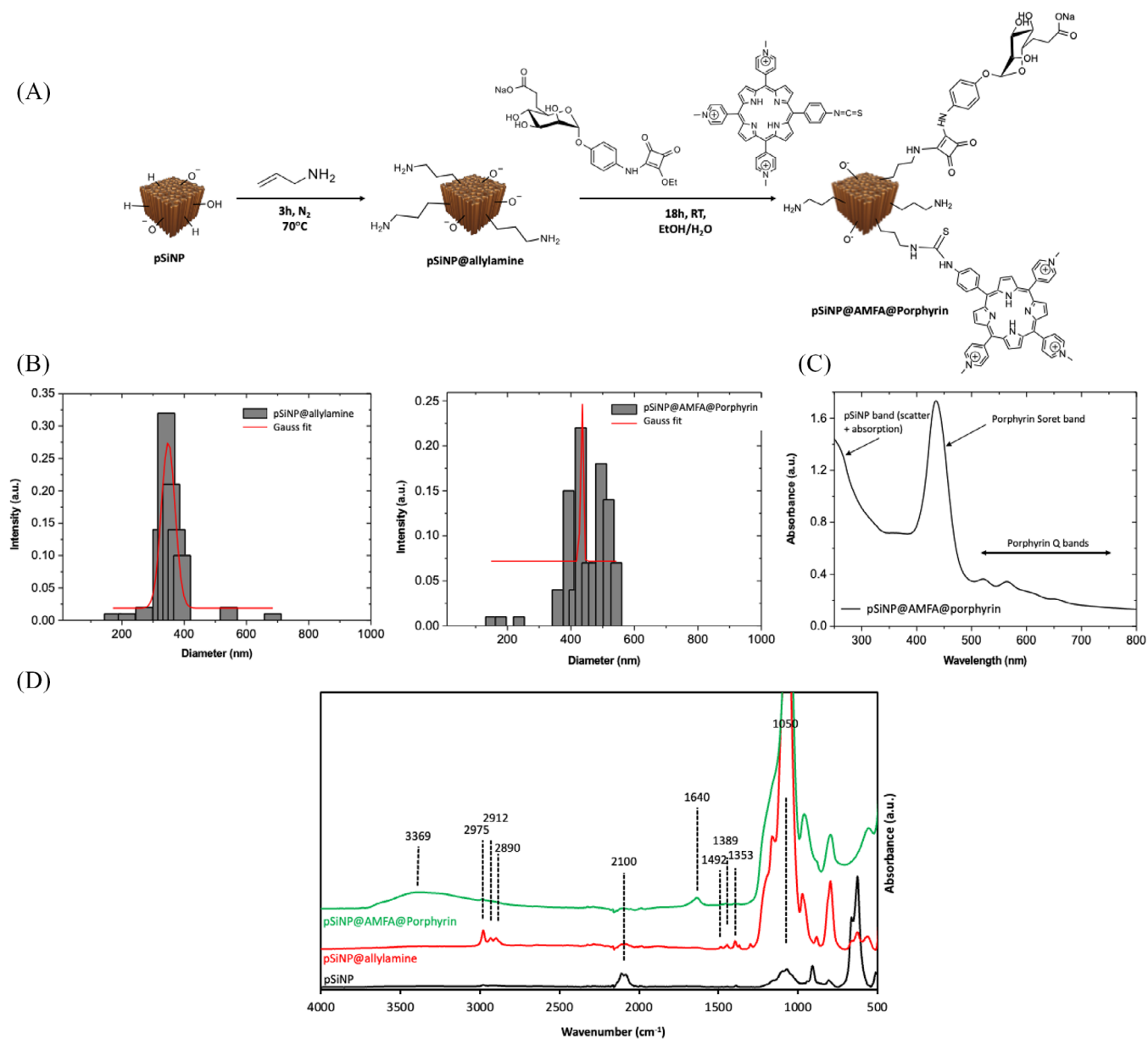


FIGURE 1 Synthesis and characterization of pSiNP formulations. A, Schematic representation of the grafting reaction of allylamine on pSiNP, and of the one-pot synthesis of pSiNP@AMFA@porphyrin. B, Dynamic light scattering (DLS) in intensity of pSiNP@allylamine and of pSiNP@AMFA@porphyrin. C, UV-vis-NIR absorption spectrum of pSiNP@AMFA@Porphyrin. The pSiNP band at low wavelength and the characteristic bands of the porphyrin (Soret band at 436 nm and the Q bands between 500 and 700 nm) are indicated on the figure. D, Infrared spectra of pSiNP (black line), pSiNP-allylamine (red line), and pSiNP@AMFA@porphyrin (green line).

already described by Chaix et al. (Figure 1A).^[28] The resulting pSiNP@allylamine showed a hydrodynamic diameter of 348 nm (Figure 1B) and a negative value of zeta potential of -23.9 ± 0.3 mV.

5-(4-iso-thiocyanatophenyl)-10,15,20-tris(4-N-1-methyl-4-pyridinio) porphyrin triiodide (porphyrin-NCS) and one AMFA, the mannose 6-carboxylate phenyl-squarate (M6CPhSq) were synthesized prior to be grafted to the pSiNP@allylamine. After the hydrosilylation step, the amine group reacted with the squarate moiety of the M6CPhSq and the thiocyanate group of the

porphyrin-NCS in a one-pot reaction, leading to a covalent attachment of both molecules on the surface of the pSiNP (Figure 1A). The obtained new product (so called pSiNP@AMFA@porphyrin) displayed an increased hydrodynamic diameter of 434 nm (Figure 1B) and a zeta potential of -26.3 ± 0.4 mV, with an optimized amount of AMFA coverage on the surface of pSiNP in order to efficiently target rhabdomyosarcoma cells.^[28] UV-vis-NIR absorption measurement of pSiNP@AMFA@porphyrin indicated the presence of the porphyrin on the pSiNP (Figure 1C).

These three formulations, namely pSiNP, pSiNP@allylamine, and pSiNP@AMFA@porphyrin were characterized by FTIR spectroscopy (Figure 1D). The intense vibration band between 1000 and 1270 cm^{-1} was assigned to the stretching vibration mode of Si–O bonds, attesting the partial oxidation of the pSiNP surface. The bands observed between 2996 and 2880 cm^{-1} and between 1500 and 1300 cm^{-1} were assigned respectively to the asymmetric and symmetric stretching vibration modes of the aliphatic carbons (ν_{CH_2}), and to the asymmetric and symmetric bending modes of C–H (δ_{CH_2}), all of them likely related to the ethanol adsorbed inside the pores of the nanoparticles. Bands corresponding to the covalent grafting of allylamine onto pSiNP were depicted in the spectrum (red line); the disappearance of the stretching band of Si–H at 2100 cm^{-1} and the increase of the ν_{CH_2} stretching vibration modes indicated that the coupling of the allylamine onto the pSiNP has certainly occurred. After the second reaction step, the covalent attachment of the porphyrin was confirmed by the formation of a band at 1640 cm^{-1} , corresponding to stretching vibration mode of C=S bond of the thiourea. The stretching vibration modes of aromatic C=C bonds around 1480 and 1300 cm^{-1} and asymmetric and symmetric stretching vibration modes of C–H between 2996 and 2893 cm^{-1} , belonging to the AMFA and the porphyrin were also observed.

In order to investigate the RMS cell targeting capability of the pSiNP by imaging, model nanoformulations incorporating AMFA and FITC were also prepared, namely pSiNP@FITC and pSiNP@AMFA@FITC. They were synthesized following the procedure described in the Experimental section and as depicted in Figure 2. The amine group of the pSiNP@allylamine reacted in a one-pot reaction with the thiocyanate group present in the FITC and with the squarate moiety of the M6CPhSq, giving rise to pSiNP@FITC and pSiNP@AMFA@FITC nanoformulations. Both pSiNP@FITC and pSiNP@AMFA@FITC presented negative values of zeta potential -29.1 ± 0.4 and -28.3 ± 0.7 mV with hydrodynamic diameters of 326 and 351 nm, respectively.

They were characterized by FTIR spectroscopy (Figure 2). The presence of the stretching vibration mode of the C=S bond in thiourea was observed at 1614 cm^{-1} . The presence of this bond indicates the successful grafting of the FITC to the pSiNP surface. The stretching vibration modes of the aromatic C=C, around 1480 and 1300 cm^{-1} , and of the asymmetric and symmetric stretching vibration modes of C–H between 2972 and 2878 cm^{-1} , belonging to the AMFA were also observed. In addition, the intense vibration band between 1000 and 1270 cm^{-1} was assigned to the stretching vibration mode of Si–O–Si bonds, due to the partial oxidation of the pSiNP surface. The large band at 3332 cm^{-1} was

assigned to the stretching vibration modes of O–H bonds from the silanol present at the oxidized pSiNP surface. Finally, colloidal stability of the nanoparticles formulations (5 mg mL^{-1}) in ethanol was observed for pSiNP, pSiNP@allylamine, pSiNP@AMFA@porphyrin, pSiNP@FITC, and pSiNP@AMFA@FITC (pictures of the nanoparticles dispersability not shown).

We have studied the targeting potential of the nanoparticles, anchored or not with AMFA, on healthy myoblasts or rhabdomyosarcoma cells. For this, cells in culture were incubated with 20 $\mu\text{g mL}^{-1}$ pSiNP@AMFA@FITC or pSiNP@FITC for 24 hours. Cells were stained with DAPI to visualize the nuclei in blue and with cell mask to highlight the membranes of the cells in red (Figure 3A). Upon light excitation at 488 nm, RD rhabdomyosarcoma cells exhibited a higher internalization potential of both nanoparticles than healthy myoblasts (Figure 3A). This is not surprising as cancer cells have a higher ability to internalize nanoparticles with a size around 100–250 nm diameter, than healthy cells. In addition, pSiNP@AMFA@FITC seemed more efficiently internalized by RD cells than pSiNP@FITC, probably due to (i) the hydrophilicity provided by AMFA and (ii) the active targeting of M6PR overexpressed by RD cells,^[27] which is the specific receptor of AMFA. Then, we have studied the two-photon excitation PDT effect of pSiNP@AMFA@porphyrin on RD cells and on healthy myoblasts (Figure 3B,C). For this, cells were incubated 5 hours with 80 $\mu\text{g mL}^{-1}$ pSiNP@AMFA@porphyrin and irradiated with NIR pulsed laser at 800 nm (Zeiss LSM 980, Chameleon laser, 3 W input, three scans of 1.43 seconds each).

Quantification of living cells (Figure 3B,C) showed that (i) irradiation without nanoparticles did not induce any significant toxicity on both cell lines, (ii) the presence of pSiNP@AMFA@porphyrin induced a slight but significant decrease in living cells, and importantly (iii) the treatment with pSiNP@AMFA@porphyrin combined with a very short laser excitation in NIR induced additional cell death of about 35% in rhabdomyosarcoma cells, while no two-photon PDT effect was observed at the same condition in healthy myoblasts (Figure 3B,C). In this PDT study, a higher concentration (80 $\mu\text{g mL}^{-1}$) was necessary to generate a significant cell death, while a short time (5 hours) was observed to be sufficient to obtain a biological effect.

Confocal microscopy experiment, using 3D reconstruction, confirmed that even after only 6 hours incubation time with Rh4 cells, another cell line of rhabdomyosarcoma, pSiNP@AMFA@FITC are more efficiently internalized than pSiNP@FITC, as highlighted by the red arrows (Figure 4) and in Videos S1 and S2 (Supporting Information).

The efficiency of internalization of pSiNP@AMFA@FITC was also studied in a kinetic study on RD

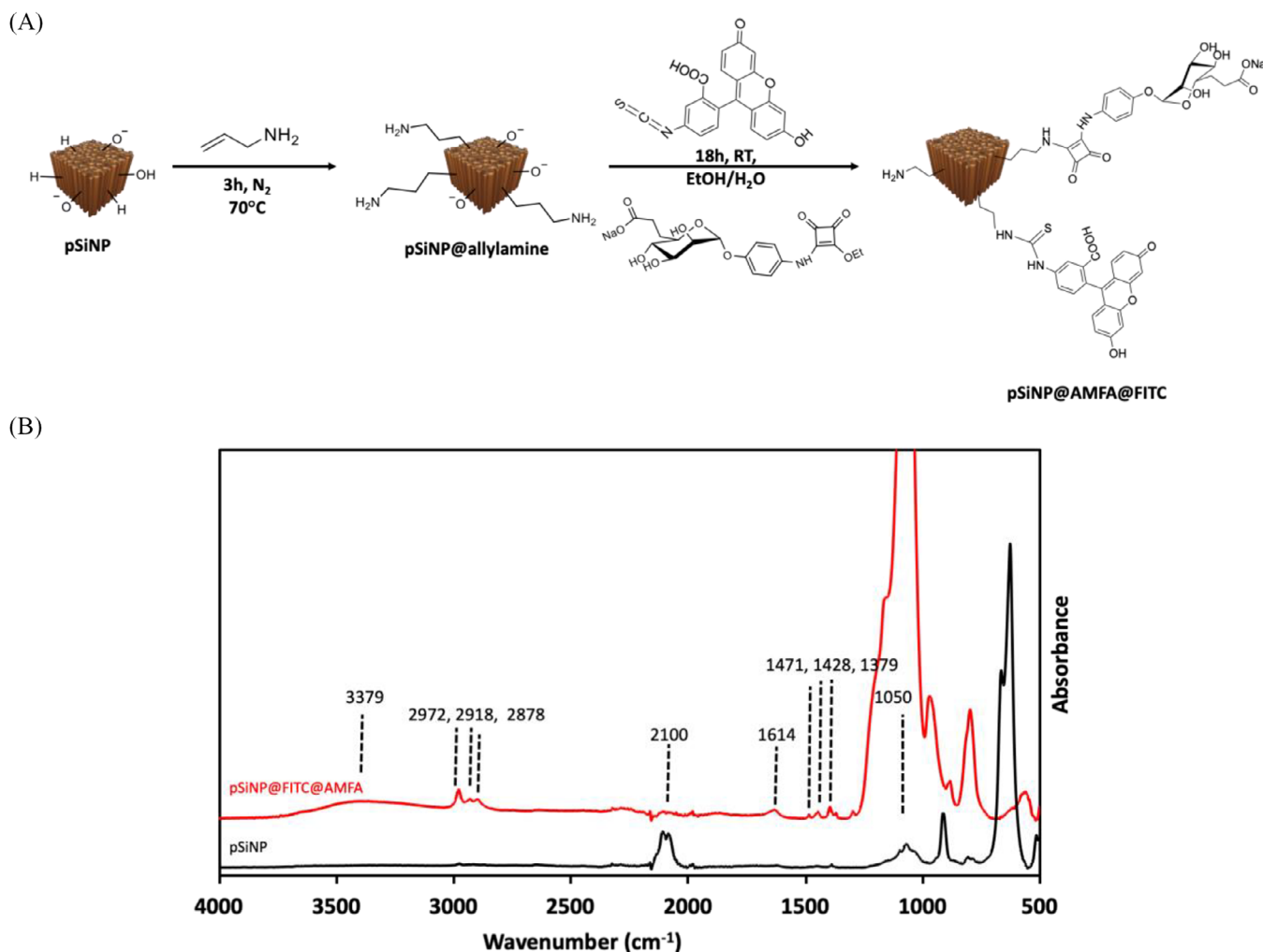


FIGURE 2 Synthesis and characterization of pSiNP formulations. A, Schematic representation of the grafting reaction of allylamine on pSiNP, and of the one-pot synthesis of pSiNP@AMFA@FITC. B, Infrared spectra of pSiNP (black line) and pSiNP@AMFA@FITC (red line).

cells. Here, cells were incubated with $40 \mu\text{g mL}^{-1}$ pSiNP@AMFA@FITC for 30 minutes, 1, 2, 5, and 24 hours (Figure 5), and then rinsed. Observation of the cells under confocal microscope indicated that pSiNP@AMFA@FITC are internalized by RD cells as a function of incubation time, with an optimum at 5 hours, and then maintained stable at least to 24 hours (Figure 5A). In addition, 3D reconstruction imaging clearly shown that the nanoparticles are internalized inside the cells (Figure 5B).

Finally, in order to confirm the involvement of an active targeting mediated by M6PR and AMFA, we have generated Rh4 M6PR knockout clones via CRISPR/Cas9 technology. The operating mode to obtain such genetically modified cells is precisely described in the Experimental Part. We observed that pSiNP@AMFA@FITC ($40 \mu\text{g mL}^{-1}$ for 24 hours) were well internalized and well dispersed in wild-type Rh4 (Rh4 WT), as previously demonstrated (Figure 4), whereas in Rh4 knockout for M6PR (Rh4 KO

M6PR), the blocking of pSiNP@AMFA@FITC endocytosis was strong (Figure 6). This demonstrated the importance of the active targeting mediated by the recognition between M6PR and AMFA to increase the internalization in rhabdomyosarcoma cells.

3 | CONCLUSION

Porous silicon nanoparticles were functionalized with AMFA and a porphyrin derivative, and their two-photon excitation photodynamic efficacy was evaluated on several RMS cell lines. The obtained data demonstrated the benefit of AMFA to target RMS cells, and confirmed the results previously shown with PMO-AMFA.^[27] As functionalized pSiNP constitute efficient cargos, offering new and promising approach for targeting, imaging, and treating RMS pediatric cancer cells.

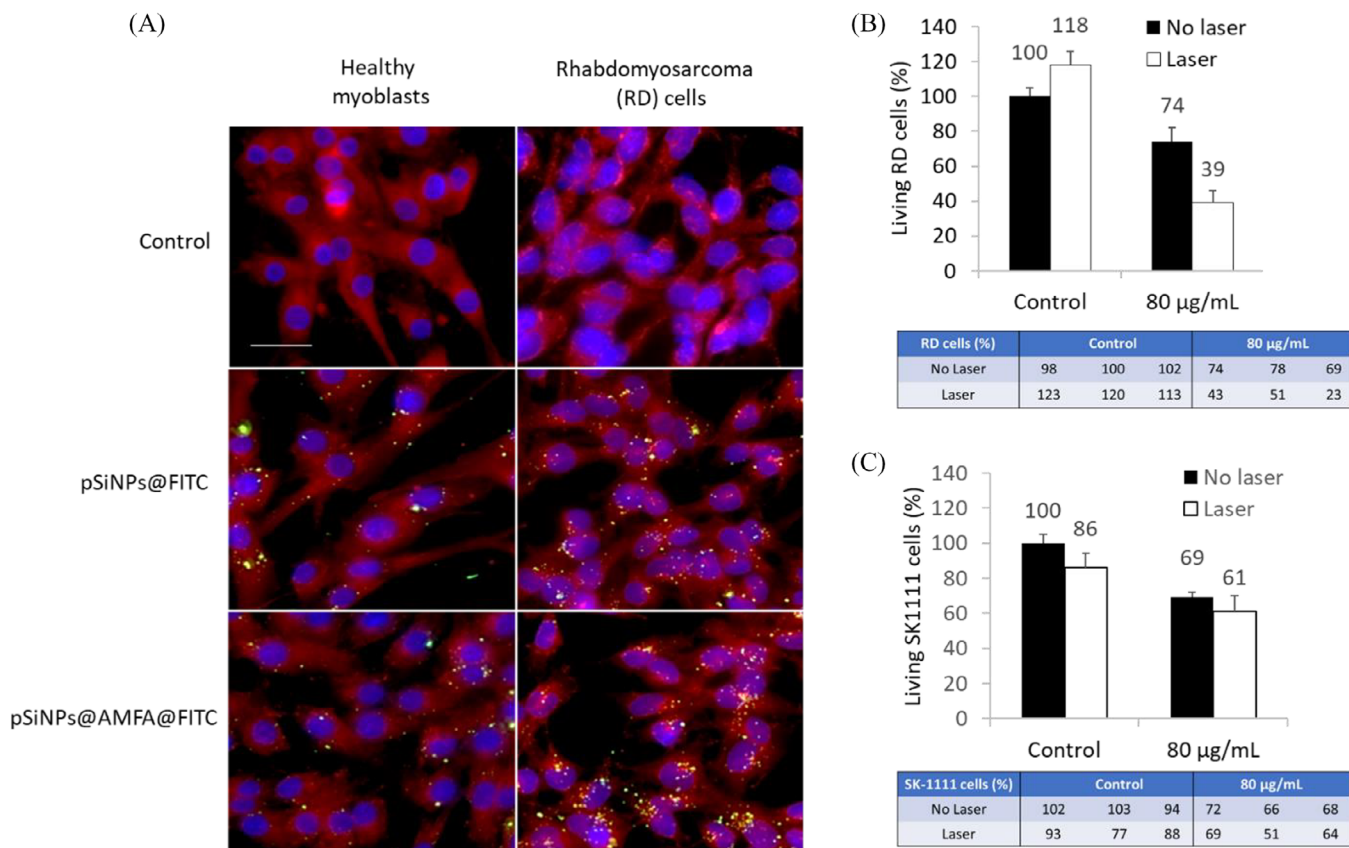


FIGURE 3 Internalization and PDT effect in healthy myoblasts and rhabdomyosarcoma cells. A, SK1111 (myoblasts) and RD (rhabdomyosarcoma) living cells were incubated with $20 \mu\text{g mL}^{-1}$ of pSiNP@AMFA@FITC or pSiNP@FITC for 24 hours. Widefield microscopy (Leica DMI4000 magnification: $40\times$), allowed the detection of nuclei stained with DAPI (blue), membranes stained with CellMask (red), and pSiNP@FITC with or without AMFA (green) after excitation at 488 nm. Scale bar = 10 μm . B, Two-photon excitation PDT ($\lambda_{\text{ex}} = 800 \text{ nm}$) on RD cells incubated 5 hours with $80 \mu\text{g mL}^{-1}$ pSiNP@AMFA@porphyrin. Bar graphs correspond to the mean of three experiments \pm standard deviation of values reported in the table below. C, Two-photon excitation PDT ($\lambda_{\text{ex}} = 800 \text{ nm}$) on SK1111 cells incubated 5 hours with $80 \mu\text{g mL}^{-1}$ pSiNP@AMFA@porphyrin. Bar graphs correspond to the mean of three experiments \pm standard deviation of values reported in the table below. For each cell type, living cells quantification was performed 48 hours after irradiation using MTT assay. * $p < 0.05$, significantly different from “No laser” (Student’s t -test).

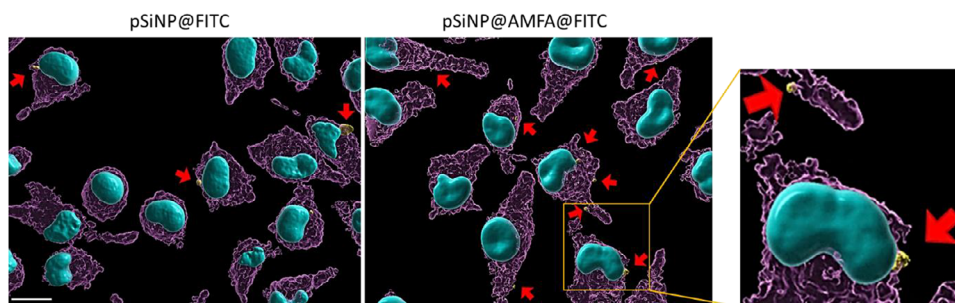


FIGURE 4 Imaging of pSiNP@FITC and pSiNP@AMFA@FITC in rhabdomyosarcoma cells. Rh4 living cells were incubated with $20 \mu\text{g mL}^{-1}$ of pSiNP@FITC or pSiNP@AMFA@FITC for 6 hours. Confocal microscope (Zeiss LSM710) imaging in 3D allowed the detection of nuclei stained with DAPI (blue), lysosomes stained with LysoTracker Deep Red (red). Nanoparticles (green) are highlighted with red arrows. Pictures 3D reconstructions were performed using Imaris software. Insert represents a magnification of a selected area.

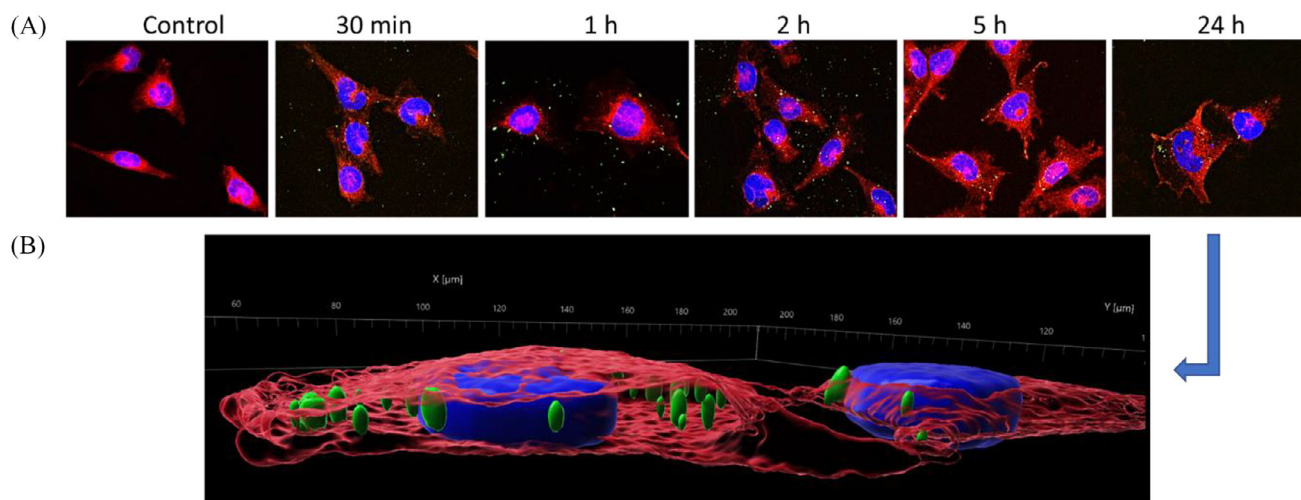


FIGURE 5 Internalization of pSiNP@AMFA@FITC in rhabdomyosarcoma cells. A, RD living cells were incubated with pSiNP@AMFA@FITC at $40 \mu\text{g mL}^{-1}$ during increasing times from 0.5 to 24 hours, and visualized with Zeiss LSM710 confocal microscope. The nuclei were stained with DAPI (blue) membrane cells were stained with CellMask (red) and pSiNP@AMFA@FITC appears in green after excitation at 488 nm. B, Three-dimensional reconstruction of the data obtained at 24 hours incubation time. Control = untreated cells. Scale bar: $10 \mu\text{m}$.

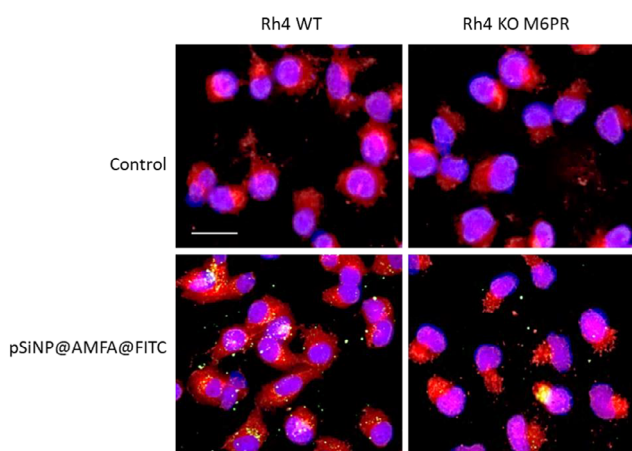


FIGURE 6 M6PR-dependent pathway for internalization of pSiNP@AMFA@FITC. Rh4 wild type or KO for M6PR were incubated with pSiNP@AMFA@FITC at $40 \mu\text{g mL}^{-1}$ for 24 hours and visualized with Leica DMI4000 widefield microscope. The nuclei were stained with DAPI (blue), cell membranes were stained with CellMask (red) and pSiNP@AMFA@FITC appears in green after excitation at 488 nm. Magnification: $40\times$. Scale bar: $10 \mu\text{m}$.

4 | EXPERIMENTAL SECTION

4.1 | Chemistry

4.1.1 | Materials

Hydrofluoric acid (HF, 48%), Allylamine (98%), FITC (90%), and Diethylether ($\geq 97.5\%$) were purchased from Sigma-Aldrich. Ethanol (EtOH, 100%) was purchased from VWR. p-[N-(2-Ethoxy-3,4-dioxocyclobut-

1-enyl)amino]phenyl 6 deoxy-7- hydroxycarbonyl- α -D-manno-heptopyranoside [M6C-PhSq] was synthesized according to the synthesis described by Bouffard et al.^[29] It was used to target the M6PR and will be called AMFA. Boron-doped p++-type Si (0.8–1.2 $\text{m}\Omega \text{ cm}$ resistivity, $\langle 100 \rangle$ orientation) was purchased from Siltronix (France).

4.2 | Analytical techniques

4.2.1 | Characterization of the pSiNP by dynamic light scattering

DLS measurements were performed in ethanol at a concentration of 1 mg mL^{-1} on a Malvern nanozetasizer instrument.

4.2.2 | Characterization of the nanoformulations by Fourier transform infrared spectroscopy

Fourier-transform infrared (FTIR) spectra were recorded on a PerkinElmer Spectrum Two (Waltham, MA, USA) spectrometer using the ATR measurement mode ($4000\text{--}400 \text{ cm}^{-1}$ range, at a resolution of 4 cm^{-1} , four repetitions).

4.2.3 | Zeta potential measurements

Zeta potential measurements were performed in water at a concentration of 1 mg mL^{-1} on a Malvern Zetasizer NanoSeries Instrument (pH 7.2 NaCl 1 mM).

4.2.4 | Characterization of the nanoformulations by UV-vis-NIR spectroscopy

UV-vis absorption spectra were recorded on a Hewlett-Packard 8453 spectrophotometer using correction factors supplied by the manufacturer.

4.2.5 | Characterization of the linkers by ^1H and ^{13}C solution NMR

^1H and ^{13}C solution NMR spectra were recorded on a Bruker AC 400 spectrometer. Chemical shifts (in δ units, ppm) are referenced to TMS using residual DMSO- d_6 ($\delta = 2.50$ ppm) resonance as the internal standard for ^1H NMR spectra, and DMSO- d_6 ($\delta = 39.52$ ppm) for ^{13}C NMR spectra.

4.2.6 | Synthesis of 5-(4-iso-thiocyanatophenyl)-10,15,20-tris(4-N-1-methyl-4-pyridinio) porphyrin triiodide

The water-soluble 5-(4-iso-thiocyanatophenyl)-10,15,20-tris(4-N-1-methyl-4-pyridinio) porphyrin trichloride was prepared according to method described by Sutton et al.^[30] Succinctly, 5-(4-acetamidophenyl)-10,15,20-tri-(4-pyridyl)porphyrin was obtained by Adler condensation. 5-(4-aminophenyl)-10,15,20-tri-(4-pyridyl)porphyrin prepared from by 5-(4-acetamidophenyl)-10,15,20-tri-(4-pyridyl)porphyrin by acid hydrolysis (HCl 5 N), was converted to 5-(4-iso-thiocyanatophenyl)10,15,20-tri-(4-pyridyl)-porphyrin then methylated by methyl iodide.

4.2.7 | Synthesis of pSiNP

Boron-doped p^{++} -type Si (0.8–1.2 m Ω cm resistivity, <1 0 0> orientation) was electrochemically etched in a 3:1 (v:v) solution of aqueous 48% hydrofluoric acid (HF):absolute ethanol. Etching was performed in a Teflon cell with a platinum ring counter electrode. A constant current of 179 mA cm^{-2} was applied for 160 seconds, and the sample was rinsed three times with absolute ethanol. The porous layer was then removed from the substrate by application of a constant current of 1.57 mA cm^{-2} for 240 seconds in an electrolyte solution containing 1:13.5 (v:v) aqueous 48% hydrofluoric acid: absolute ethanol. After three rinses with absolute ethanol, the porous layer was placed in ethanol in a glass vial. After degassing the sample for 20 minutes under a nitrogen stream, the porous silicon film was fractured by ultrasonication during 21 hours (Ultrasonic cleaner Fisher Transsonic

TI-H-10). The largest particles were removed by spinning them down by centrifugation at 3000 rpm for 3 minutes. In order to remove the smallest particles, the solution was finally centrifuged at 14,000 rpm for 30 minutes. The pellet was then redispersed in absolute ethanol.

4.2.8 | Allylamine grafting onto pSiNP by hydrosilylation

Freshly prepared pSiNP were centrifuged at 14,000 rpm for 10 minutes in ethanol, then 44.5 mg of pSiNP were redispersed in 13 mL of allylamine and reacted for 3 hours at 70°C under inert atmosphere. After the reaction, the aminated pSiNP (pSiNP-NH₂) were centrifuged at 14,000 rpm for 20 minutes and washed five times with absolute ethanol to remove the allylamine adsorbed onto their surface. The pSiNP-NH₂ were finally redispersed in 10 mL ethanol.

4.2.9 | One-pot reaction between the pSiNP-NH₂, the cationic porphyrin, and the AMFA

For the simultaneous grafting of the cationic porphyrin and the AMFA, 330 μL of a solution of AMFA at 16 mM in 1:1 (v:v) ethanol/water mixture and 167 μL of a solution of the cationic porphyrin at 1 mg mL^{-1} in ethanol were added to 10 mg of suspension of the pSiNP-NH₂. The reaction was performed under stirring during 18 hours at room temperature. The obtained nanoparticles were centrifuged at 14,000 rpm during 20 minutes and rinsed twice with absolute ethanol, twice with deionized water, twice with absolute ethanol, twice with diethylether, twice with absolute ethanol, producing 8 mg of pSiNP@AMFA@porphyrine in absolute ethanol.

4.2.10 | FITC grafting on pSiNP-NH₂

Twenty milligram of pSiNP-NH₂ were redispersed in 1 mL of absolute ethanol. 0.5 mg of FITC in 1 mL of absolute ethanol was added to the solution and the mixture was stirred at RT overnight. The nanoparticles were centrifuged at 14,000 rpm for 20 minutes giving rise to 14 mg of pSiNP@FITC in absolute ethanol.

4.2.11 | One-pot reaction between the pSiNP-NH₂, the FITC, and the AMFA

For the simultaneous grafting of the FITC and the AMFA, 500 μL of a solution of AMFA at 16 mM in 1:1 (v:v) ethanol/water mixture and 250 μL of a solution

of the FITC at 1 mg mL⁻¹ in ethanol were added to a 15 mg of suspension of the pSiNP-NH₂. The reaction was performed under stirring overnight at room temperature. The obtained nanoparticles were centrifuged at 14,000 rpm during 20 minutes and rinsed twice with absolute ethanol, twice with deionized water, producing 12 mg of pSiNP@AMFA@FITC in absolute ethanol.

4.3 | Biology

4.3.1 | Cell lines

The rhabdomyosarcoma (RMS) cell lines RMS, Rh4, and RD, were kindly provided by Prof. Beat Schäfer (University Children's Hospital of Zurich) and cultivated in a humidified 5% CO₂ incubator at 37°C in Dulbecco's modified Eagle's medium/GlutaMAX (Thermo Fisher Scientific) supplemented with 10% FBS (10270106, Thermo Fisher Scientific) and 1% penicillin/streptomycin (4-01F00-H, Bioconcept). Primary human healthy myoblasts from Cook MyoSite were cultured in Skeletal Muscle Cell Growth Medium (C-23060, PromoCell) supplemented with Skeletal Muscle Cell Growth Medium SupplementMix (C-39365, PromoCell), in a humidified 5% CO₂ incubator at 37°C. Cells were tested negative for mycoplasma. Trypsin (0.25% w/v) containing EDTA (0.02% w/v) was used to detach cells from the bottom of flasks (25300054, Thermo Fisher Scientific).

4.3.2 | Two-photon excitation for PDT

Cancer and healthy cells were seeded into a 384 multi-well glass-bottomed plate (thickness 0.17 mm) with a black polystyrene frame at a concentration of 1000 cells per well in 50 µL of culture medium, and allowed to grow for 24 hours. After seeding, dispersed pSiNP@AMFA@Porph were added on cells at a concentration of 80 µg mL⁻¹ for 5 hours. After this incubation, cells were submitted or not to laser irradiation with the LSM 980 live confocal microscope (Carl Zeiss Microscope, Chameleon laser, 3 W power input) at 800 nm by three scans of 1.43 seconds duration in four different areas of the well with a focused laser at a maximum laser power. The laser beam was focused by a microscope objective lens (Carl Zeiss 10×/0.3 EC Plan-Neofluar). After 2 days, the MTT assay was performed as previously described and was corrected according to the following formula: Abs "No laser" - 2 × (Abs "No laser" - Abs "Laser"). Values are the mean of three experiments and error bars represent standard deviation.

4.3.3 | Fluorescent microscopy

For the internalization analysis by confocal or widefield microscopy, 10,000 or 20,000 RMS cells (Rh4, RD) or healthy myoblast were seeded per well on a 8-well chamber cover glass slides (80826, Ibidi) in full growth medium and allowed to adhere to the surface for 24 hours in a 37°C humidified incubator with a 5% CO₂ atmosphere. The next day, the cells were incubated or not with 20 µg mL⁻¹ or 40 µg mL⁻¹ of pSiNP@FITC or pSiNP@AMFA@FITC for different time-points. After incubation, cells were washed with PBS, loaded during 7 minutes at 37°C with Deep Red CellMask (C10046, ThermoFisher) or LysoTracker Deep red (L12492, ThermoFisher) to respectively stain the cell membranes or the lysosomes, and fixed with 2% PFA (043368.9 M, Thermo Fisher Scientific) for 15 minutes at 37°C. The cells were then washed three times for 5 minutes with Tris saline buffer (TBS) and DAPI in TBS was added for 2 minutes prior mounting with a chamber-compatible medium (50001, Ibidi). The samples were imaged using the Leica_DMI4000 for widefield microscopy and the Zeiss LSM710 for confocal microscopy. 3D reconstructions were made using the Imaris software (Oxford Instruments).

4.3.4 | M6PR-KO cell lines generation by CRISPR/Cas9

Rh4 M6PR knockout clones were generated via CRISPR/Cas9 technology. A pair of complementary single-strand oligonucleotides encoding the sgRNA sequence for M6PR knockout were selected by using the Graphical User Interface for DNA Editing Screens (GUIDES), available at guides.sanjanalab.org (**AAACCTGTGACCCTCTGGTGGAGGC** and **AAACTTTGACAGACGGCGATCTCGC**) and used in a tandem strategy. An Esp3I restriction site was added. The sgRNA were then annealed and cloned into the lentiGuide-Puro plasmid a gift from Feng Zhang (Addgene plasmid # 52963)^[31] via Esp3I (ER0451, Thermo Fisher Scientific) restriction and T4 ligation (15224017, Thermo Fisher Scientific). Cas9⁺ mCherry⁺ Rh4 cells, previously reported,^[32] were transiently transfected with the construct using the JetOptimus transfection reagent (117-01, Polyplus Transfection) according to the manufacturer's recommendations. Clonal cell populations were obtained by the dilution limit method. Cells were selected with puromycin (1 µg mL⁻¹) and single-cell cloning was performed with selected cells on 96-well plates. The M6PR knockout was confirmed by sequencing and looking at the cell surface expression of M6PR in WT and KO Rh4 cell lines using flow cytometry.

4.3.5 | Flow cytometry

To confirm the loss of M6PR in the M6PR KO cell line, 250,000 WT or KO Rh4 cells were stained with 2.5 μ L of M6PR PE anti-human (IP-315-T100, EXBIO) or the corresponding IgG1 PE isotype control (IP-632, EXBIO) in 100 μ L of FACS buffer (PBS with 0.5% BSA) in the dark and at 4°C for 30 minutes. After three washes with FACS buffer, the samples were acquired using a Cytoflex flow cytometer (Beckman Coulter). The data were analyzed with FlowJo (BD Biosciences).

4.3.6 | Statistical analysis

Statistical analysis was performed using the Student's *t*-test to compare paired groups of data. A *p*-value of <0.05 was considered to be statistically significant.

ACKNOWLEDGMENTS

“Bernese Foundation for Children and Young Adults with Cancer / Berner Stiftung für krebskranke Kinder und Jugendliche” and the Mach-Gaensslen Foundation are gratefully acknowledged for financial support. The authors gratefully acknowledge the University of Montpellier and the imaging facility MRI, member of the national infrastructure France-BioImaging infrastructure supported by the French National Research Agency (ANR-10-INBS-04, «Investments for the future»). This publication is part of the Special Issue organized by COST Action NETPORE (CA20126), supported by COST (European Cooperation in Science and Technology).


CONFLICT OF INTEREST STATEMENT

JR is currently an employee of Novartis Pharma Basel.

DATA AVAILABILITY STATEMENT

The data that support the findings of this study are available from the corresponding author upon reasonable request.

ORCID

Frédérique Cunin  <https://orcid.org/0000-0003-4624-8418>

REFERENCES

1. M. Schindler, F. N. Belle, M. A. Grotzer, N. X. von der Weid, C. E. Kuehni, G. Swiss Paediatric Oncology, *Int. J. Cancer* **2017**, *140*, 62.
2. C. D. M. Fletcher, E. H. Baldini, J. Y. Blay, A. Gronchi, A. J. Lazar, C. Messiou, R. E. Pollock, S. Singer, WHO Classification of Tumours, in *Soft Tissue and Bone Tumours* (Ed. T.W.C.o.T.E. Board), Vol. 5th., IARC Press, Lyon 2020, pp. 201–215.
3. F. G. Barr, L. M. Smith, J. C. Lynch, D. Strzelecki, D. M. Parham, S. J. Qualman, P. P. Breitfeld, *J. Mol. Diagn.* **2006**, *8*, 202.
4. D. Williamson, E. Missiaglia, A. de Reynies, G. Pierron, B. Thuille, G. Palenzuela, K. Thway, D. Orbach, M. Lae, P. Freneaux, K. Pritchard-Jones, O. Oberlin, J. Shipley, O. Delattre, *J. Clin. Oncol.* **2010**, *28*, 2151.
5. S. Malempati, D. S. Hawkins, *Pediatr. Blood Cancer* **2012**, *59*, 5.
6. L. Tramsen, K. Bochennek, M. Sparber-Sauer, E. Salzmann-Manrique, M. Scheer, T. Dantonello, A. Borkhardt, U. Dirksen, A. Thorwarth, J. Greiner, M. Ebinger, J. Weclawek-Tompol, R. Ladenstein, G. Ljungman, E. Hallmen, T. Lehrnbecher, E. Koscielniak, T. Klingebiel, *Cancers (Basel)* **2023**, *15*, 2050.
7. M. E. van de Velde, M. H. van den Berg, G. J. L. Kaspers, F. C. H. Abbink, J. W. R. Twisk, I. M. van der Sluis, C. van den Bos, M. M. van den Heuvel-Eibrink, H. Segers, C. Chantrain, J. van der Werff Ten Bosch, L. Willems, R. R. L. van Litsenburg, *Cancer Med.* **2021**, *10*, 8172.
8. J. A. Punyko, A. C. Mertens, J. G. Gurney, Y. Yasui, S. S. Donaldson, D. A. Rodeberg, R. B. Raney, M. Stovall, C. A. Sklar, L. L. Robison, K. S. Baker, *Pediatr. Blood Cancer* **2005**, *44*, 643.
9. A. A. Owosho, P. Brady, S. L. Wolden, L. H. Wexler, C. R. Antonescu, J. M. Huryn, C. L. Estilo, *Pediatr. Hematol. Oncol.* **2016**, *33*, 383.
10. S. Triarico, A. Romano, G. Attina, M. A. Capozza, P. Maurizi, S. Mastrangelo, A. Ruggiero, *Int. J. Mol. Sci.* **2021**, *22*, 4112.
11. S. N. Bhatia, X. Chen, M. A. Dobrovolskaia, T. Lammers, *Nat. Rev. Cancer* **2022**, *22*, 550.
12. T. M. Allen, P. R. Cullis, *Adv. Drug Deliv. Rev.* **2013**, *65*, 36.
13. H. A. Yousefi Rizi, D. Hoon Shin, S. Yousefi Rizi, *Iran J. Public Health* **2022**, *51*, 226.
14. S. Bayda, M. Hadla, S. Palazzolo, P. Riello, G. Corona, G. Toffoli, F. Rizzolio, *Curr. Med. Chem.* **2018**, *25*, 4269.
15. S. Yang, M. Wallach, A. Krishna, R. Kurmasheva, S. Sridhar, *J. Clin. Med.* **2021**, *10*, 1437.
16. T. C. Pham, V. N. Nguyen, Y. Choi, S. Lee, J. Yoon, *Chem. Rev.* **2021**, *121*, 13454.
17. C. A. Robertson, D. H. Evans, H. Abrahamse, *J. Photochem. Photobiol. B* **2009**, *96*, 1.
18. S. S. Lucky, K. C. Soo, Y. Zhang, *Chem. Rev.* **2015**, *115*, 1990.
19. Y. Shen, A. J. Shuhendler, D. Ye, J. J. Xu, H. Y. Chen, *Chem. Soc. Rev.* **2016**, *45*, 6725.
20. N. T. Chen, K. C. Tang, M. F. Chung, S. H. Cheng, C. M. Huang, C. H. Chu, P. T. Chou, J. S. Souris, C. T. Chen, C. Y. Mou, L. W. Lo, *Theranostics* **2014**, *4*, 798.
21. S. J. Soenen, P. Rivera-Gil, J. M. Montenegro, W. J. Parak, S. C. De Smedt, K. Braeckmans, *Nano Today* **2011**, *6*, 446.
22. E. B. Ehlerding, F. Chen, W. Cai, *Adv. Sci. (Weinh)* **2016**, *3*, 1500223.
23. E. J. Anglin, L. Cheng, W. R. Freeman, M. J. Sailor *Adv. Drug Deliv. Rev.* **2008**, *60*, 1266.
24. J. H. Park, L. Gu, G. von Maltzahn, E. Ruoslahti, S. N. Bhatia, M. J. Sailor, *Nat. Mater.* **2009**, *8*, 331.
25. L. Xiao, L. Gu, S. B. Howell, M. J. Sailor, *ACS Nano* **2011**, *5*, 3651.
26. E. Secret, M. Maynadier, A. Gallud, A. Chaix, E. Bouffard, M. Gary-Bobo, N. Marcotte, O. Mongin, K. El Cheikh, V. Hugues, M. Auffan, C. Frochot, A. Morere, P. Maillard, M. Blanchard-Desce, M. J. Sailor, M. Garcia, J. O. Durand, F. Cunin, *Adv. Mater.* **2014**, *26*, 7643.
27. M. Daurat, C. Nguyen, S. Dominguez Gil, V. Sol, V. Chaleix, C. Charnay, L. Raehm, K. El Cheikh, A. Morere, M. Bernasconi, A. Timpanaro, M. Garcia, F. Cunin, J. Roessler, J. O. Durand, M. Gary-Bobo, *Biomater. Sci.* **2020**, *8*, 3678.

28. A. Chaix, K. El Cheikh, E. Bouffard, M. Maynadier, D. Aggad, V. Stojanovic, N. Knezevic, M. Garcia, P. Maillard, A. Morere, M. Gary-Bobo, L. Raehm, S. Richeter, J. O. Durand, F. Cunin, *J. Mater. Chem. B* **2016**, *4*, 3639.
29. E. Bouffard, C. Mauriello Jimenez, K. El Cheikh, M. Maynadier, I. Basile, L. Raehm, C. Nguyen, M. Gary-Bobo, M. Garcia, J. O. Durand, A. Morere, *Int. J. Mol. Sci.* **2019**, *20*, 2809.
30. O. J. C. J. M. Sutton, N. Fernandez, R. W. Boyle *Bioconjugate Chem.* **2002**, *13*, 249.
31. N. E. Sanjana, O. Shalem, F. Zhang, *Nat. Methods* **2014**, *11*, 783.
32. A. Timpanaro, C. Piccand, D. Dzhumashev, S. Anton-Joseph, A. Robbi, J. Moser, J. Rossler, M. Bernasconi, *J. Exp. Clin. Cancer Res.* **2023**, *42*, 293.

SUPPORTING INFORMATION

Additional supporting information can be found online in the Supporting Information section at the end of this article.

How to cite this article: S. Dominguez-Gil, R. Sala, V. Morel, C. Nguyen, K. E. Cheikh, A. Morère, J.-O. Durand, J. Rössler, M. Bernasconi, F. Cunin, M. Gary-Bobo, *Nano Select* **2024**, *5*, 2400004.
<https://doi.org/10.1002/nano.202400004>